FISEVIER

Contents lists available at ScienceDirect

## Innovative Food Science and Emerging Technologies

journal homepage: www.elsevier.com/locate/ifset





# Optimization of complex food formulations using robotics and active learning

Deborah Becker <sup>a,\*</sup>, Christophe Schmitt <sup>a</sup>, Lionel Bovetto <sup>a</sup>, Cornelia Rauh <sup>b</sup>, Christopher McHardy <sup>b</sup>, Christoph Hartmann <sup>a,b</sup>

- <sup>a</sup> Nestlé Research, Nestlé Institute of Material Sciences, Vers-Chez-Les-Blanc, Lausanne CH-1000 26, Switzerland
- b Institute of Food Technology and Food Chemistry, Technische Universität Berlin, Berlin 14195, Germany

ARTICLE INFO

Keywords:
Automated robotic platform
Machine learning
Multiobjective optimization
Whey protein isolate

#### ABSTRACT

The creation and optimization of formulated products represents a major challenge for science and industry in the food sector. Thereby, different raw materials are mixed and processed to meet predefined and often competing targets. During this procedure, applied experimental campaigns not only require expert knowledge, but, depending on the complexity, also cause a high consumption of resources and costs. In the present work, a fully automized milli-fluidic laboratory driven by the Thomsen sampling efficient multiobjective optimization (TSEMO) algorithm was designed. The methodology was successfully applied to optimize the aggregation process of a liquid formulation consisting of whey protein isolate, NaCl and CaCl<sub>2</sub>. Within 48 h 90 experiments could be performed without human intervention, resulting in a Pareto front formed by a set of 18 optimal recipes. It is thus a successful demonstration of an actively learning, self-driving food formulation process.

## 1. Introduction

Formulation strategies are used in various applications and stages during the development of food products, recipes, or ingredients. Thereby the formulated product can serve as a raw material for products of greater value or be the final product itself. For both cases, the formulation process can be described as a simple concept including the mixing of components with the objective to obtain a certain functionality. In reality, formulated product design represents a complex and challenging task, once considering the possible interaction of the components at the molecular level and the influence of the process conditions. Additionally, factors such as consumer preferences, costs and sustainability often need to be taken into account (Pathania, Bhatia, & Tiwari, 2021). The ultimate objective of any formulation development, no matter of the application, is to generate a product that performs according to the intended targets. Therefore, the main goal in formulation optimization is to identify the best level of each component, their effect and, if required, the critical processing variables (Arteaga, Li-Chan, Vazquez-Arteaga, & Nakai, 1994).

The optimization procedure requires often labor-intensive experiments, as well as the involvement of specialists with extensive experience regarding the product under consideration. Although experiments

and expert knowledge can often lead to success, this approach reaches its limits when developing products with increased complexity (e.g., more than four input variables). It is almost impossible to screen all potential ingredients, their interaction and modification during a process, not even considering possible influencing parameters of the manufacturing technologies and operating conditions. Resulting empirical or semi-empirical models provide therefore in some cases only an insufficiently accurate prediction.

One approach to address this limitation is the implementation of more system-aided techniques. In the case of multiple targets so called multi-objective optimization algorithms (MOOAs) are used. The relation between input and output is hereby described by objective functions, whereby one objective function exists for each objective, i.e., the targeted properties. The objective functions can be divided into fast or slow to compute (i.e., cheap or expensive) and analytic or Black-Box (Mueller, 2022). A Black-box function is a function, for which neither the analytical form (e.g., linear or quadratic) nor any gradient information is known. When solving an expensive Black-box optimization problem, surrogate models and active learning are therefore implemented. Surrogate models are data driven and computationally cheap approximations of the unknown expensive objective function (Booker, Dennis Jr, Serafini, Torczon, & Trosset, 1999). Active learning is a subfield of

E-mail address: deborah.becker@rd.nestle.com (D. Becker).

 $<sup>^{\</sup>ast}$  Corresponding author.

machine learning, using sequential sampling, and the learning algorithm can choose the data from which it learns (Settles, 2009). The sequential sampling technique is thereby based on two concepts: exploration and exploitation. While exploration aims to reduce uncertainties by covering poorly sampled areas in the design space, exploitation focuses on already highly sampled regions to refine the predictive model locally. The active learning algorithm determines the next sample point by trading-off both concepts. This technique, combined with the integration of system knowledge during the sample generation, leads to better approximations of the system by avoiding under- or oversampling.

The optimization process starts with an initial training data set to build the surrogate model. This model is used in a next step to select the next sample point in the experimental space to be evaluated. Subsequently, the data set is updated, and the surrogate model trained with the gained new information. These steps, surrogate model training and selection/ evaluation of new data point, are repeated until a predefined stop criterion is reached, e.g., the maximum number of samples (Mueller, 2022). The multiple objectives in formulation optimization problems are typically opposing, what makes it rarely possible to find a unique solution being overall optimal. Instead, the aim of MOOAs is to identify a set of solutions that represent an optimal trade-off between the different objectives, termed as Pareto set or Pareto front (Censor, 1977). Since such a Pareto set is often infinite and the entire front cannot be generated analytically, the aim of MOOAs is to find an approximation with a finite number of points.

In the field of chemical engineering, machine learning (ML)-based modeling could be applied successfully to solve nontrivial formulation optimization problems. Current studies in the field of chemical engineering implemented the Thompson sampling efficient multi-objective algorithm (TSEMO) for multi-target optimization with continuous input and output variables (Cao et al., 2021; Clayton et al., 2020; Knox, Parkinson, Wilding, Bourne, & Warren, 2022; Schweidtmann et al., 2018).

Besides accurate models with high prediction power, the generation of a large number of repeatable and robust data is a key element for an efficient and fast optimization of formulated products. However, the creation of large data sets usually involves routine operations, which imply a high risk of human influence and error during routine operations. Often, environmental conditions, notably the temperature, also have a major impact on the results. These challenges can be overcome by adopting automated high-throughput experiments using robotics. A successful adoption of such systems can be found in chemical and pharmaceutical engineering (Fricke et al., 2013; Salley, Keenan, Long, Bell, & Cronin, 2020).

Formulations containing proteins are an example of complex optimization problems. Whether as an ingredient for protein-enriched foods or as an additive to improve the properties of a final product, proteins are of major interest in the development of new products. The functional application of whey protein isolate (WPI) is particularly reasoned by the water-binding and gelling capacity and their ability to stabilize interfaces in foams and emulsions (Boland, 2011). Due to these properties WPI is used to achieve desired structural and sensory characteristics in a wide range of food products. However, whey protein in its native form is not commonly used, as it has a compact globular structure and a small molecular weight (Fitzsimons, Mulvihill, & Morris, 2008). Instead, the use of polymerized whey protein (PWP) is preferred. In function of the applied heat treatment the molecular structure of the protein is hereby modified including unfolding, denaturation, and the formation of stable soluble protein aggregates. The latter are referred to as whey protein aggregates (WPA). Size, shape, and structure of the WPAs after the preprocessing are depending on the heating protocol, the protein concentration, the pH and the concentration and type of the salts added (Nicolai, Britten, & Schmitt, 2011). One procedure to generate such WPAs is the salt-induced cold-set aggregation. The whey protein is in a first step thermally processed to prepare a heat-denatured protein solution containing small and soluble primary aggregates with filamentous type structure and irreversible bonds (Baussay, Le Bon, Nicolai, Durand, & Busnel, 2004; Bryant & McClements, 1998). Once cooled, this step is followed by the induction of further aggregation by adding salt. The salt ions decrease hereby the electrostatic repulsion by neutralizing the charged surface of the protein molecules (Petit, Herbig, Moreau, & Delaplace, 2011; Schmitt, Bovay, Rouvet, Shojaei-Rami, & Kolodziejczyk, 2007).

A commonly used method for monitoring the aggregation process is the measurement of turbidity. Hereby an increasing turbidity can be detected due to the formation of aggregates that are large enough to scatter light (approx. > 100 nm) (Bryant & McClements, 2000). The turbidity depends on the number of aggregates as well as on their size and scattering efficiency (McClements & Keogh, 1995). For solutions with a protein concentration below the critical gelation concentration  $C_g$  the aggregation can be monitored as well with viscosity measurements. Hereby the viscosity increases due to the larger effective volume fraction of the aggregates compared to the individual molecules (Vardhanabhuti & Foegeding, 1999).

At the present stage of formulation processing, it is necessary to constantly adapt the ingredient concentrations in order to maintain consistent product quality and properties. In this study, a milli-fluidic robotic platform was therefore developed for fully automated dosing, mixing and analyzes of a liquid formulation. The platform was linked to an optimization algorithm TSEMO, forming a closed-loop system to optimize the salt induced cold-set aggregation process of whey protein isolate regarding two continuous targets, i.e. viscosity and turbidity. The chosen formulation has a moderate complexity and is scientifically well researched. Therefore, the objective of this work was to use this formulation as a proof of concept in order to apply such optimization systems to more complex problems in the future.

## 2. Materials and methods

## 2.1. Case study and materials for stock solutions

The studied and optimized case was a formulation consisting of a whey protein isolate (BiPRO 9500, lot JE 0148–20-420) and two salts, i. e., sodium chloride (ACS reagent,  $\geq 99\%$ ) and calcium chloride (calcium chloride dihydrate, ACS reagent,  $\geq 99\%$ ). All raw materials came in dry form and were dissolved in deionized water with a conductivity of 1.2  $\mu S/cm$ . The WPI powder contains on a dry basis 98% protein, whereby the composition is about 80% beta-lactoglobulin and 20% alphalactalbumin in a very native and soluble state.

## 2.2. Experimental space

The limits of the experimental space were set based on literature references, with the aim to prevent any gel formation in the samples (Baussay et al., 2004; Purwanti et al., 2011). Accordingly, the following lower and upper bounds were determined: 1–6% w/w WPI, 0–90 mM NaCl and 0–6 mM CaCl<sub>2</sub>. The resolution of the dosing of each ingredient, i.e., the concentration increase per dosing step, was 0.06% w/w for WPI, 3 mM for NaCl and 0.2 Mm for CaCl<sub>2</sub>.

## 2.3. Preparation of stock solutions

In a first step a WPI stock solution of 10% w/w was prepared by dispersing the WPI powder in deionized water. Bacterial growth was prevented by adding Sodium Azide (0.02%) to the solution. The dispersion was then stirred at room temperature (20–23  $^{\circ}$ C) for two hours and left at 4  $^{\circ}$ C for 16 h to ensure complete hydration. The measured pH of the untreated WPI solution after stirring was 6.9–6.93. In a second step, the WPI solution was preheated without stirring in a water bath to 60  $^{\circ}$ C, followed by a heating procedure in an oil bath at 85  $^{\circ}$ C for 15 min with gentle stirring (40 rpm). The time it took to reach 85  $^{\circ}$ C was 10 min. After these heat treatments, the solution was cooled in

ice water to 30 °C, which took around 5 min. The salt solutions were each mixed with deionized water and stirred at room temperature until they were completely dissolved. Before each experiment run, the solutions were preheated to 30 °C.

## 2.4. Robotic platform

The robotic platform was designed as a continuous flow through system in a milli-fluidic scale to reduce the needed sample quantity and therefore waste. In addition, in-line and real-time measurement technologies for the aggregation monitoring were implemented to avoid any human intervention. The platform can be divided into three layers as represented in Fig. 1. The basis forms the component layer, which consists of all hardware elements, i.e., sensors and actuators. Centerpiece of the robotic system is the core layer, containing the control software for interfacing with the hardware elements and enabling data generation. The complete sequence of an experiment is stored in the experimental layer, which interfaces with the core layer in order to perform the desired commands. Not part of the robotics platform, but connected to the experimental layer, is the analytical layer, which contains the optimization algorithm (see section 2.5).

## 2.4.1. Component layer

To ensure a constant operating temperature of 30  $^{\circ}$ C all components of the component layer were designed or selected in terms of their dimensions such that they fitted under a heatingamber CERTOMAT® HK from *Sartorius*. Fig. 2 shows a picture of the complete experimental setup. A supplementary overview of all components and a scheme in top view of the robotic platform are given in Fig. 3.

Each reservoir of stock solution or deionized water was coupled with an assembly of peristaltic pumps driven by stepper motors, with a resolution of 0.1 g per step. In order to achieve a higher accuracy and to avoid errors during the dosing, the quantities dispensed by the motorpump assembly were counter-checked by a balance. All stock solutions were directly dispensed into a reaction vial, with a total quantity of each sample fixed to 15 g. The vial was made of glass and held by a 3D printed stand which enabled a stable positioning on the balance. An outlet at the bottom allowed complete emptying, controlled by a normally closed micro electric solenoid valve. To detect the temperature of the mixed solution a temperature sensor was places in the vial. A complete mixing of the dosed stock solutions was ensured by implementing a micro surface stirrer adjusted to a speed of 60 rpm. The mixing time was set to

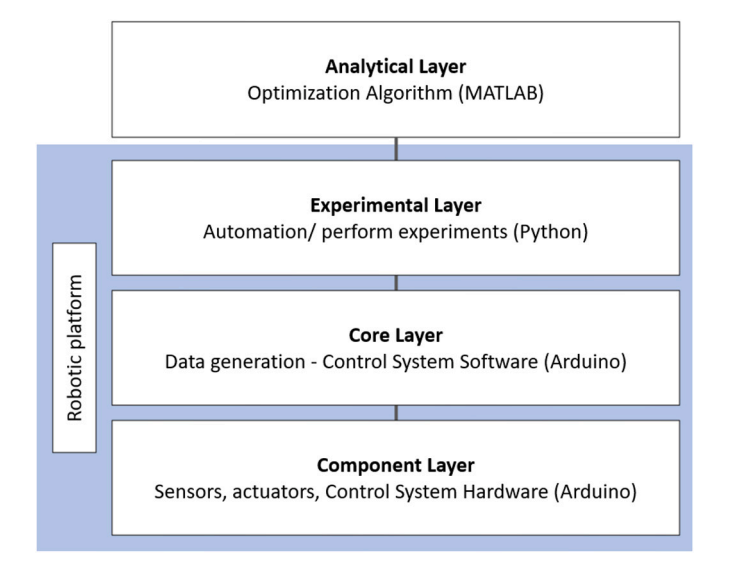


Fig. 1. Hardware and software architecture of the robotic system split into three distinct layers. The fourth layer represents the coupled optimization step.

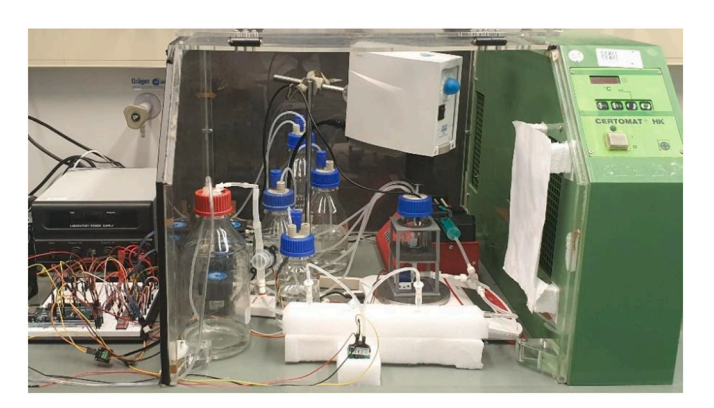


Fig. 2. Photo of the complete experimental setup.

20 min and followed by in-line measurements of viscosity and turbidity (in Nephelometric Turbidity Units NTU).

The design of the implemented in-line viscometry system follows the concept of a capillary viscometer. Based on the principles of the Hagen-Poiseuille equation, the viscosity can hereby be determined by measuring the pressure drop in a cylindrical pipe at a constant laminar flow. With  $\Delta p$  representing the pressure drop,  $\eta$  the dynamic viscosity, l the length of the measurement section, Q the volumetric flow rate and r the pipe radius, the notation of this fluidic law is the following [Eq. (1)]:

$$\eta = \frac{\pi \cdot r^4 \cdot \Delta p}{8 \cdot O \cdot I} \tag{1}$$

The resulting experimental set-up is illustrated in Fig. 4.

An accurate, constant and pulsation free flow was generated by the syringe pump (LA-110 from LANDGRAF HLL). A passive non-return valve with three luer lock connections controlled the varying flow directions of withdrawing and pumping. The geometry of the custom-built glass-capillary was determined by the following factors: the spatial capacity under the heating chamber, the necessary conditions of laminar and fully developed flow, the expected measurement range of the pressure drop and the prevention of any interaction of fluid particles and capillary wall. Taking all these aspects into account, the total length of the capillary was 28 cm, with 10 cm for the inlet section of the hydrodynamic flow stabilization and 15 cm for the measurement section itself. With an inner diameter  $d_i$  of 0.84 mm and a flow rate of 15 ml/min, the chosen geometry resulted in a Reynolds number of Re = 385, representing therefore a laminar flow. As a reference, the values of viscosity and density  $\rho$  were set to those of water. With the given geometry and flow conditions, the shear rate was 4296.4  $s^{-1}$ . The capillary was positioned horizontally at the same height as the syringe and had a connection for the differential pressure sensor at the beginning and end of the measuring section. A pressure differences in the range of 0-100 mbar could be measured with the pressure sensor module DRMOD-I<sup>2</sup>C from B + B SENSORS. In order to test the functionality of the developed capillary viscometer, the viscosity of water at different temperatures and flow rates was measured and compared to literature values. In addition, nine samples with different WPI and salt concentration were tested in parallel with the capillary viscometer and modular compact rheometer from Anton Paar using a double-gap system. Since a shear rate of 4296.4 s<sup>-1</sup> is too high to be replicated with the double-gap system without causing turbulence, the highest feasible shear rate was set (around 500 s<sup>-1</sup>) and the data was fitted with the Sisko model to calculate the infinite shear viscosity  $\eta_{\infty}$ , according to Eq. 2.

$$\tau = c \cdot \dot{\gamma}^p + \eta_\infty \cdot \dot{\gamma} \tag{2}$$

Herein,  $\tau$  is the shear stress,  $\dot{\gamma}$  the shear rate, c the consistency index and p the power law index. This model specifically describes the behavior at high shear rates (Mezger, 2020). Measurement results of the capillary were below those of the rheometer, due to the strong deviation

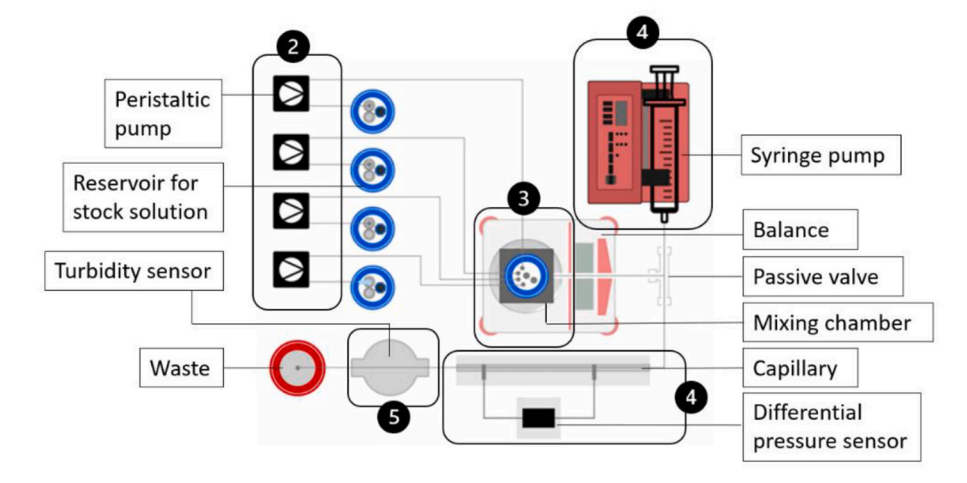


Fig. 3. Scheme of the subgroups 2) the dosing system, 3) the reaction chamber, 4) viscometry system and 5) turbidity sensor.

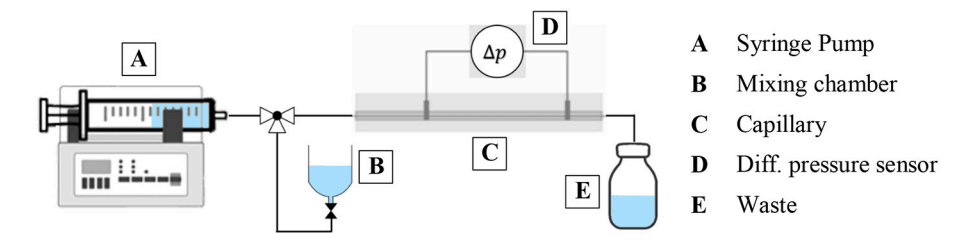


Fig. 4. Experimental set-up of the capillary viscometer.

of the shear rate, but for all samples systematically in line. Therefore, differences in the viscosity of each sample could be detected with high reliability, which was critical for the proof of concept.

To measure the turbidity a TST-10 turbidity sensor was integrated in the system. The sensor operates according to the transmitted light method, whereby the intensity of the transmitted light through the sample is measured in an angle of 180°. Installed vertically in the system, air bubble free measurement was enabled, as these were rising to the top and thus out of the relevant measuring section before the measurement started. To minimize the influence of the surrounding light, the housing was additionally shielded with aluminum foil (not shown in Fig. 2). The sensor was calibrated with a dilution series based on Formazin Standard *TURB4000* from *Sigma-Aldrich*.

To prevent any cross contamination with the former sample, all tubes and devices were cleaned twice with deionized water after each experiment.

The accuracy of the pump and motor assembly was determined by calculating the deviation between the target dosage value and the actual performed dosing quantity for all experiments, detected by the balance. In addition, the overall platform accuracy was tested by dosing and analyzing a randomly selected sample composition four times. The results are listed in Table 1.

The step size of the dosage of 0.1 g was not exceeded by any assembly. The deviations of the viscosity and turbidity measurements were also small enough to enable detection of variations between different sample compositions and therefore prevent a distortion of the optimization process.

#### 2.4.2. Core and experimental layer

Apart from two components (the balance and the syringe pump) the control for the entire system was realized through Arduino (Arduino Mega 2560). The balance and the syringe pump were programmed internally and therefore only required data transfer via RS232. The exact procedure of an experiment was managed by a custom written program in Python.

## 2.5. TSEMO algorithm

In constant exchange with the experimental layer was the analytical layer. The latter consists of an optimization algorithm named "Thompson sampling efficient multi-objective optimization" (TSEMO) (Bradford, Schweidtmann, & Lapkin, 2018). The TSEMO algorithm solves expensive black-box problems by using Gaussian processes (GPs) as surrogates for each objective function (more information about GPs can be found in Schulz, Speekenbrink, and Krause (2018)). To build the initial GPs a primary training dataset needs to be provided, which was done by using Latin hypercube sampling. An initial number of 30 experiments was chosen according to the 10xd rule of thumb, with d representing the number of input variables, which are the concentrations of WPI, NaCl and CaCl<sub>2</sub> (Loeppky, Sacks, & Welch, 2009).

During the optimization procedure the GPs are trained, and single-objective Thompson Sampling (TS) is used to sample distinct functions from the independent GPs using spectral sampling. In a next step the approximate Pareto set of each sampled function is determined by implementing the generic algorithm NSGA II, a fast and elitist algorithm performing non-dominated and crowding distance sorting to obtain a

**Table 1**Accuracy of the dosing system (from 94 experiments) and sample analysis (from four repetitions).

	Assembly 1 WPI [g]	Assembly 2 NaCl [g]	Assembly 3 CaCl <sub>2</sub> [g]	Viscosity [μPas]	Turbidity [NTU]
Average deviation	+0.04	+0.03	+0.05	$\pm 7.1$	±5

Pareto front (Deb, Pratap, Agarwal, & Meyarivan, 2002). The obtained front contains all possible points for evaluating the objective function in the following iteration. To choose finally the next sampling point from this candidate set, the hypervolume quality indicator is used. Hereby the hypervolume improvement of each point of the candidate set, once added to the current Pareto front, is calculated. The point that gives the largest improvement is chosen as the next evaluation point.

## 2.6. Closed-loop optimization procedure

The optimization problem presented here comprised three input variables, concentration of WPI, NaCl and  $CaCl_2$  converted as quantity in g and was simultaneously optimized with respect to the two objectives turbidity and viscosity. To create a non-trivial problem with conflicting objectives, the turbidity was to be maximized and the optimization problem resulted in the following [Eq. (3)]:

$$minimize[-NTU, \eta]$$
 (3)

With respect to the application of a whey protein-salt mixture, this optimization targeted a formation of a large number of small aggregates. A general scheme of the workflow is represented in Fig. 5. The robotic platform and optimization algorithm were coupled and formed a closed-loop system. At each iteration a sample was mixed from the previously prepared stock solutions and analyzed regarding viscosity and turbidity. These measurement data, as well as weighed dosed quantities served as input for the linked TSEMO algorithm which generated a suggestion for a new sample composition based on all prior experiments. In the following iteration step the stock solutions were dosed based on this suggestion and the entire procedure was repeated until the defined maximum number of iterations was reached. The stop criterion was set to a maximum number of 60 iterations. Analytical and experimental layer communicated via a constantly updating file.

## 3. Results

The 30 initial data points were analyzed with the robotic platform and used to initiate the coupled TSEMO algorithm. The optimization process itself comprised 60 iteration steps, with these being divided into two runs of 30 samples and a duration of 16 h each run. This division was intended to prevent any change in the properties of the WPI stock solution when stored too long at 30  $^{\circ}\text{C}$ . The process was started immediately after preparation of the stock solutions, continued to run overnight, and stopped automatically after the maximum number of iterations was reached. On average, the calculation time of each new predicted sample point took between 10 and 15 s. The results of the optimization are shown in.

Fig. 6, including the 30 initial sample points and the 60 sample points predicted by the TSEMO algorithm. A moderate increase in viscosity can be seen on the left side, followed by a strong rise in the values on the right side. A Pareto front consisting of 18 solutions was formed, containing 17 points generated by the algorithm and one data point

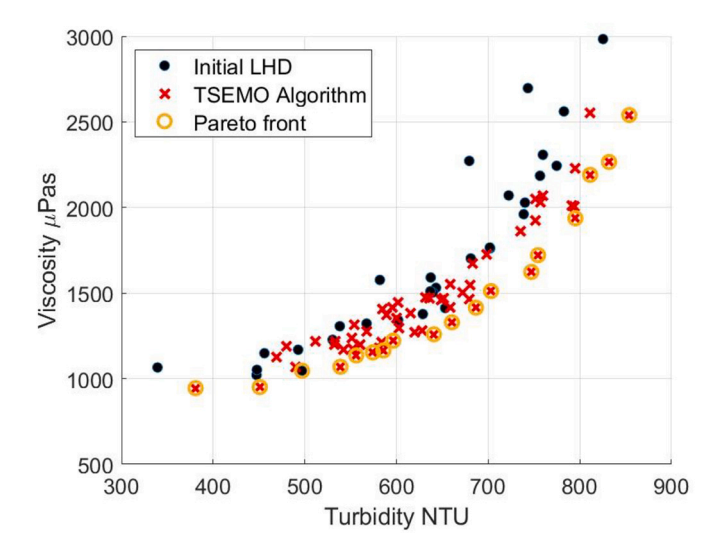


**Fig. 6.** Results of the multi-objective optimization aiming to minimize the viscosity and maximize the turbidity of a formulation consisting of WPI, NaCl and CaCl<sub>2</sub>. The initial LHS size was 30 and the TSEMO algorithm conducted 60 additional experiments.

resulting from the initial data set. All data points of the pareto front are listed in Table 2. The optimum viscosity value, i.e., the minimum, was 944.66  $\mu$ Pas with a turbidity value of 380.79 NTU. Conversely, a

**Table 2**Set of non-dominated solutions that build the pareto front of the optimized data. The maximal value for the turbidity was achieved in iteration 56 and the minimal viscosity value was measured in iteration 33.

	Iteration	WPI [% <i>w</i> /w]	NaCl [mM]	CaCl <sub>2</sub> [mM]	Viscosity [μPas]	Turbidity [NTU]
Training data	26	1.56	39.16	5.84	1046.32	496.94
	33	0.99	0.00	1.45	944.66	380.79
	36	1.17	15.50	5.89	951.17	450.83
	40	2.04	30.66	5.97	1135.71	556.08
	41	2.24	26.29	5.98	1165	585.8
	44	2.45	78.84	2.77	1221.93	596.42
	46	2.19	78.45	3.18	1153.53	574.18
	48	3.53	5.91	3.59	1414.61	686.65
Optimization	49	2.35	3.25	5.97	1259.11	640.8
data	52	5.23	0.00	5.35	2190.8	811.18
uata	53	4.96	65.42	4.93	2265.84	831.88
	54	1.70	17.90	5.43	1069.82	538.84
	55	4.24	87.16	5.81	1936.95	795.1
	56	5.11	82.91	5.40	2540.11	853.92
	57	4.06	35.90	5.52	1721.27	754.39
	58	3.50	5.43	5.75	1511.87	703.09
	59	3.50	87.29	6.01	1623.38	747.03
	60	3.11	58.73	1.09	1329.23	660.45

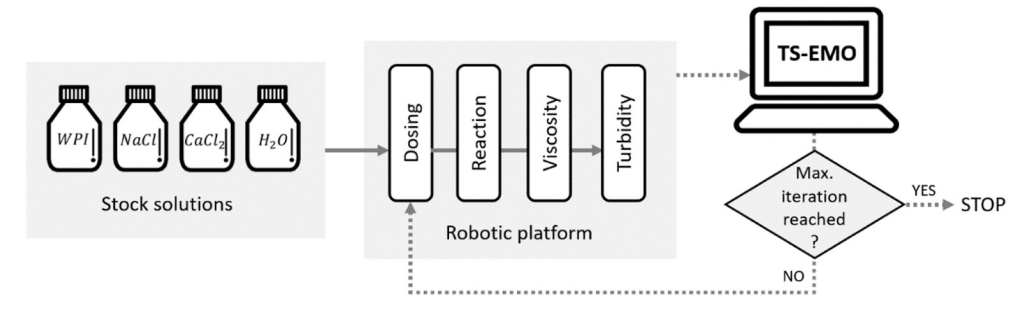


Fig. 5. Scheme of the closed-loop optimization workflow where continuous lines represent the material flow, whereas the information flow is represented by dotted lines.

viscosity of 2540.11  $\mu Pas$  was measured at the optimum turbidity value of 853.92 NTU. These values point out the trade-off between the two objectives, thus an increase in turbidity is always correlated with an increase in viscosity.

The TSEMO algorithm also reports the values of the final hyperparameters, presented in Table 3. Hyperparameters are included in the surrogate GP models and provide qualitative process information. The hyperparameters  $\lambda_d$  correspond to the input variables and reveal the relevance of each. A lower value of  $\lambda_d$  indicates a greater contribution to the objective (Bradford et al., 2018).

The final hyperparameters of the decision variables show, that WPI has the highest contribution to both objectives, closely followed by CaCl<sub>2</sub> in the case for the turbidity. NaCl, on the other hand, has a less significant impact.

In order to gain further information about the effect of each ingredient, the turbidity and viscosity values are visualized as a function of the sample composition in Figs. 7 and 8 respectively.

As indicated in Fig. 7, the sample with the lowest measured turbidity value was composed of 1% w/w WPI and 0 mM NaCl, which is the limit of the lower bound for both ingredients. The concentration of CaCl $_2$  was hereby 1.45 mM. The sample having the highest turbidity value was mixed out of 5.1% w/w WPI, 83 mM NaCl and 5.4 mM CaCl $_2$ . The turbidity profile of all points along the z-axis indicates that varying the concentration of NaCl between 0 and 90 mM has little effect on this objective. In contrast, an increase of the WPI concentration results in a large increase of the turbidity. The CaCl $_2$  concentration also shows an increasing effect on the turbidity of the sample. In addition, the distribution of data points in the design space reveals the trend with which the algorithm has chosen the sample composition. The positioning of the points on the WPI-CaCl $_2$  plane shows a diagonal progression from [0% w/w, 0 mM] to [6% w/w, 6 mM], whereby the concentration of NaCl increases the more the sample is located near the latter point.

In Fig. 8, the measured viscosity values are represented. The point with the lowest viscosity also had the lowest turbidity and thus the composition was identical: 1% w/w WPI, 0 mM NaCl and 1.45 mM CaCl $_2$ . The highest measured viscosity value was at  $2554.26~\mu Pas$  with a sample composition of 5.4% w/w WPI, 50 mM NaCl and 6.1 mM CaCl $_2$ . When considering the color gradient of all data points, the concentration of WPI shows a strong influence on the viscosity. The influence of CaCl $_2$  is not clearly detectable from this plot. There seems to be an enhancing effect with an increase of CaCl $_2$  concentration, but the color pattern is not consistent especially in the range of higher CaCl $_2$  concentrations. The concentration of NaCl shows a low effect on the viscosity.

## 4. Discussion

The visualization of the results in Figs. 7 and 8 does not give an obvious indication of the correlations between the components of the formulation and the respective objective. This shows that even the noncomplex system chosen here cannot be considered as trivial. By means of the information obtained by the hyperparameters, a reduction of complexity is possible with NaCl not being further considered as an influencing factor.

In Fig. 9a, the turbidity is plotted as a function of the protein concentration, including the range of CaCl<sub>2</sub> concentration in form of a scatter plot. Darker points in blue indicate a low salt concentration, while light point in yellow indicate a high concentration. A clear correlation between the WPI concentration and the turbidity values can be

**Table 3** The hyperparameters  $\lambda_d$  of the GP models for each objective after 60 iterations.

	Turbidity	Viscosity
$\lambda_{WPI}$	29.65	10.93
$\lambda_{NaCl}$	56.99	31.09
$\lambda_{CaCl_2}$	30.04	18.88

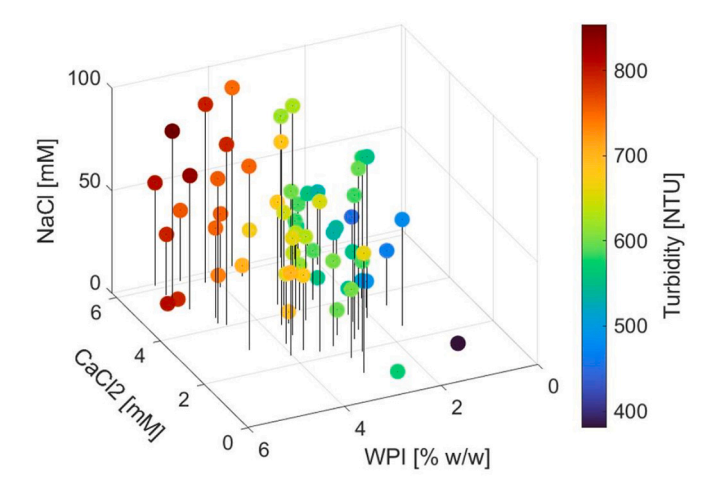


**Fig. 7.** Scatter plot visualizing the dependency of the turbidity on the three ingredients of the studied formulation, showing the 60 optimization sample points.

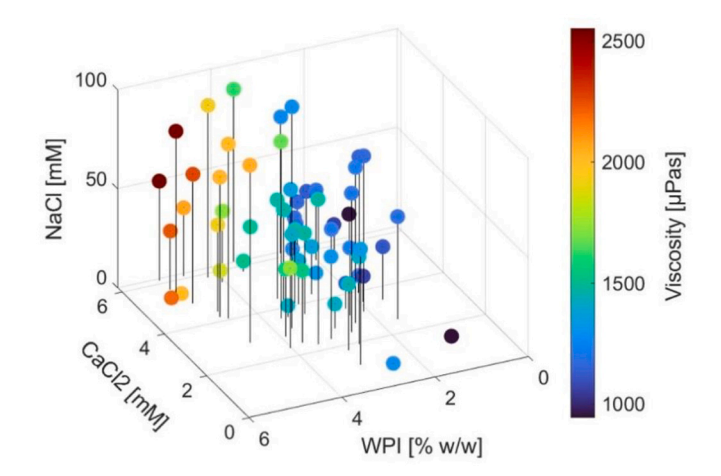


**Fig. 8.** Scatter plot visualizing the dependency of the viscosity on the three ingredients of the studied formulation, showing the 60 optimization sample points.

detected, characterized by a strong increase of the turbidity at WPI concentrations between 1 and 4%~w/w. The color gradient, representing the different CaCl<sub>2</sub> concentrations, reveals once more the influence of the salt addition. At the same level of WPI concentration, a higher salt addition leads to an increase in turbidity. This effect seems to be more pronounced for samples with a higher protein content. Fig. 9b shows the viscosity as a function of the WPI concentration. The viscosity increases exponentially with the protein concentration. The influence of CaCl<sub>2</sub> is less pronounced here and only detectable when having WPI concentrations above 4.5% w/w in the sample.

The following conclusions can be drawn from the graphical illustrations:

- 1) As indicated by the hyperparameters in Table 3, the WPI concentration has the strongest effect on both objectives. Turbidity as well as viscosity increase with increasing protein concentration, but a different course of the correlation is observed. While the viscosity increases exponentially with increasing WPI addition, the trend of turbidity shows an attenuation of the increase at WPI concentrations >3.5% w/w.
- The addition of CaCl<sub>2</sub> has an increasing effect on turbidity when comparing samples with the same WPI concentration. The effect

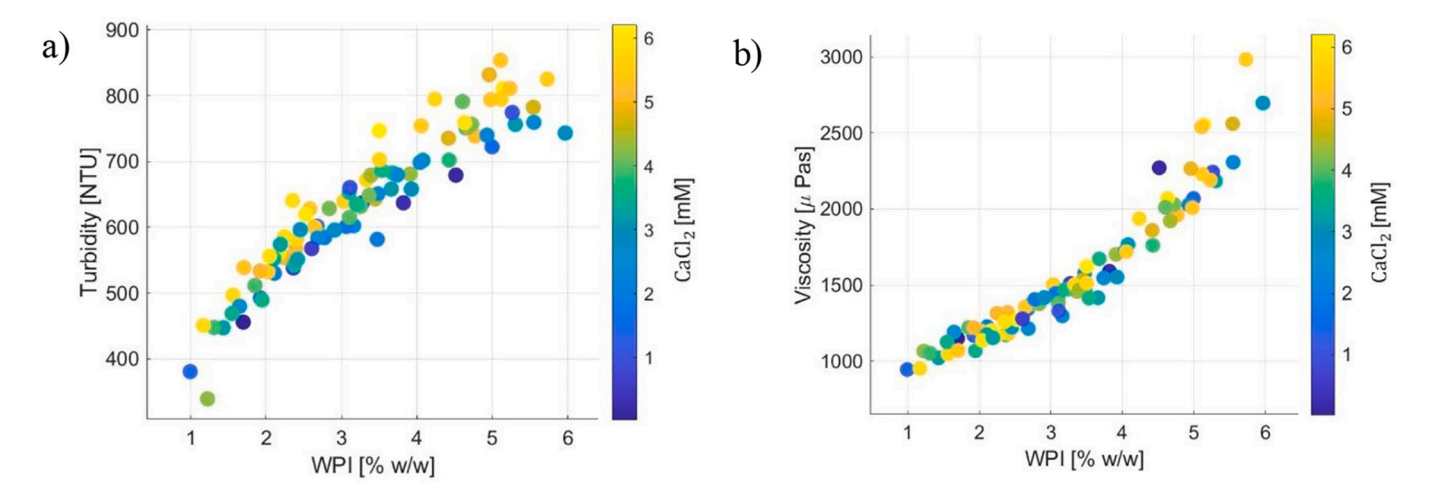


Fig. 9. Scatter plots presenting a) the turbidity and b) the viscosity as a function of the WPI concentration. The visualization of the corresponding CaCl<sub>2</sub> concentration of each sample point is included by a colormap.

increases with increasing WPI concentration. An influence on viscosity is not so clearly detectable and if so, then only in areas of high WPI concentration ( $> 4.5\% \ w/w$ ). These results are as well in correlation with the hyperparameters, which revealed a higher relevance of WPI compared to CaCl<sub>2</sub>, especially for the viscosity.

3) No effect on both objectives is detectable for the studied range of NaCl (0-90 mM). Also in this case, hyperparameters and experimental data come to the same conclusion.

That both objectives increase with increasing WPI concentration is consistent with observations given in literature. Inthavong, Kharlamova, Nicolai, and Chassenieux (2016) studied the effect of fractal aggregates from heated  $\beta$ -lactoglobulin solutions on the viscosity and reported an exponential increase of the viscosity with the protein concentration for a given aggregate size. In addition, the increase was steeper for larger aggregates due their lower density (Inthavong et al., 2016). As the turbidity depends on the volume fraction of the protein, it is therefore increasing with a higher WPI concentration. With CaCl2 addition, the electrostatic repulsion between the primary filament protein aggregates is shielded, resulting in larger aggregates. Those larger aggregated filaments scatter light more effectively than the primary filaments, which causes an increase in turbidity (McClements & Keogh, 1995). The increase in turbidity at higher CaCl2 concentrations (as seen in Fig. 9a) is therefore due formation of larger aggregates. The influence of CaCl<sub>2</sub>, hence formation of large aggregates, seems to be particularly pronounced above a WPI concentration of about 3.5–4.5% w/w. Both plots in Fig. 9 show larger deviations between samples with low and high CaCl<sub>2</sub> content, starting from these values. The effect on the aggregation rate and particle size of the monovalent salt NaCl is much less strong, compared to the divalent salt CaCl<sub>2</sub>. The latter promotes the aggregation faster and at lower concentrations, due to the higher valency of the counterion and therefore greater screening power (Bryant & McClements, 2000; Jeyarajah & Allen, 1994). In the case of mixed salt addition, the bivalent cation determines furthermore the aggregation characteristics (Kuhn & Foegeding, 1991). The upper bound of 90 mM for NaCl used in this study might not be high enough to show an effect on the aggregation.

## 5. Conclusion

In conclusion a fully automated closed-loop system for the optimization of liquid formulations could be developed, by coupling robotic experiments with a machine learning algorithm. This time- and resource-saving methodology enabled the identification of a set of

optimal solutions without human intervention. The outcome shows the great potential of implementing active learning and automation during the development of food products and food ingredients, especially at the early stages. The gained knowledge about the prevailing effects in complex systems can be derived, and used to guide further research, reduce complexity and support the transition from laboratory scale to production scale.

#### **Author statement**

**Deborah Becker:** Methodology, Software, Investigation, Visualization, Validation, Writing – Original Draft.

**Christophe Schmitt:** Expertise on Protein Science, protein aggregation.

**Lionel Bovetto:** Expertise on Protein Science, raw materials expertise.

**Cornelia Rauh:** Academic *Co-Supervision*, scientific interpretation, laboratory resources.

**Christopher McHardy**: Supervision of experimental design and data acquisition, scientific interpretation.

**Christoph Hartmann:** Conceptualization & Hypothesis, Methodology, Supervision, scientific interpretation, manuscript writing & review.

## **Funding**

This research did not receive any specific grant from funding agencies in the public, commercial, or not-for-profit sectors.

## **Declaration of Competing Interest**

The authors declare that they have no conflicts of interest to this work and no known competing financial interests or personal relationships that could have appeared to influence the work reported in this paper.

## Data availability

Data can be made available upon request, pending approval by research partners.

## References

Arteaga, G. E., Li-Chan, E., Vazquez-Arteaga, M. C., & Nakai, S. (1994). Systematic experimental designs for product formula optimization. *Trends in Food Science & Technology*, 5, 243–254. https://doi.org/10.1016/0924-2244(94)90017-5

- Baussay, K., Le Bon, C., Nicolai, T., Durand, D., & Busnel, J. P. (2004). Influence of the ionic strength on the heat-induced aggregation of the globular protein betalactoglobulin at pH 7. International Journal of Biological Macromolecules, 34, 21–28. https://doi.org/10.1016/j.ijbiomac.2003.11.003
- Boland, M. (2011). Whey proteins. In G. O. Phillips, & P. A. Williams (Eds.), Chapter 3. Handbook of food proteins (pp. 30–55). Woodhead Publishing Series in Food Science, Technology and Nutrition, Woodhead Publishing. https://doi.org/10.1533/ 9780857093639.30.
- Booker, A. J., Dennis, J. E., Jr., Serafini, D. B., Torczon, V., & Trosset, M. W. (1999). A rigorous framework for optimization of expensive functions by surrogates. Structural Optimization, 17, 1–13. https://doi.org/10.1007/BF01197708
- Bradford, E., Schweidtmann, A. M., & Lapkin, A. (2018). Efficient multiobjective optimization employing Gaussian processes, spectral sampling and a genetic algorithm. *Journal of Global Optimization*, 71, 407–438. https://doi.org/10.1007/ s10898-018-0609-2
- Bryant, C., & McClements, D. (2000). Influence of NaCl and CaCl2 on cold-set gelation of heat-denatured whey protein. *Journal of Food Science*, 65, 801–804. https://doi.org/ 10.1111/j.1365-2621.2000.tb13590.x
- Bryant, C. M., & McClements, D. J. (1998). Molecular basis of protein functionality with special consideration of cold-set gels derived from heat-denatured whey. *Trends in Food Science & Technology*, 9, 143–151. https://doi.org/10.1016/S0924-2244(98)
- Cao, L., Russo, D., Felton, K., Salley, D., Sharma, A., Keenan, G., ... Lapkin, A. (2021). Optimization of formulations using robotic experiments driven by machine learning DoE. Cell Reports Physical Science, 2. https://doi.org/10.1016/j.xcrp.2020.100295. Article 100295
- Censor, Y. (1977). Pareto optimality in multiobjective problems. Applied Mathematics and Optimization, 4, 41–59. https://doi.org/10.1007/BF01442131
- Clayton, A. D., Schweidtmann, A. M., Clemens, G., Manson, J. A., Taylor, C. J., Niño, C. G., ... Bourne, R. A. (2020). Automated self-optimisation of multi-step reaction and separation processes using machine learning. *Chemical Engineering Journal*, 384. https://doi.org/10.1016/j.cej.2019.123340. Article 123340.
- Deb, K., Pratap, A., Agarwal, S., & Meyarivan, T. (2002). A fast and elitist multiobjective genetic algorithm: NSGA-II. *IEEE Transactions on Evolutionary Computation*, 6, 182–197. https://doi.org/10.1109/4235.996017
- Fitzsimons, S. M., Mulvihill, D. M., & Morris, E. R. (2008). Segregative interactions between gelatin and polymerised whey protein. *Food Hydrocolloids*, 22, 485–491. https://doi.org/10.1016/i.foodhyd.2007.01.005
- Fricke, J., Pohlmann, K., Jonescheit, N. A., Ellert, A., Joksch, B., & Luttmann, R. (2013). Designing a fully automated multi-bioreactor plant for fast DoE optimization of pharmaceutical protein production. *Biotechnology Journal*, 8, 738–747. https://doi. org/10.1002/bjot.201200190
- Inthavong, W., Kharlamova, A., Nicolai, T., & Chassenieux, C. (2016). Structure and flow of dense suspensions of protein fractal aggregates in comparison with microgels. Soft Matter, 12, 2785–2793. https://doi.org/10.1039/C5SM02893K
- Jeyarajah, S., & Allen, J. C. (1994). Calcium binding and salt-induced structural changes of native and preheated beta-lactoglobulin. *Journal of Agricultural and Food Chemistry*, 42, 80–85. https://doi.org/10.1021/jf00037a012
- Knox, S. T., Parkinson, S. J., Wilding, C. Y. P., Bourne, R. A., & Warren, N. J. (2022). Autonomous polymer synthesis delivered by multi-objective closed-loop optimization. *Polymer Chemistry*, 13, 1576–1585. https://doi.org/10.1039/ D2PY00040G

- Kuhn, P. R., & Foegeding, E. A. (1991). Mineral salt effects on whey protein gelation. Journal of Agricultural and Food Chemistry, 39, 1013–1016. https://doi.org/10.1021/ if00006a001
- Loeppky, J., Sacks, J., & Welch, W. (2009). Choosing the sample size of a computer experiment: A practical guide. *Technometrics*, 51, 366–376. https://doi.org/ 10.1198/TECH.2009.08040
- McClements, D. J., & Keogh, M. K. (1995). Physical properties of cold-setting gels formed from heat-denatured whey protein isolate. *Journal of the Science of Food and Agriculture*, 69, 7–14. https://doi.org/10.1002/jsfa.2740690103
- Mezger, T. (2020). The rheology handbook: For users of rotational and oscillatory rheometers (5th ed.). Hannover, Germany: Vincentz Network. https://doi.org/10.1515/ 9783748603702
- Mueller, J. (2022). Optimizing expensive black-box simulations. Lawrence Berkeley National Laboratory, Center for Computational Sciences and Engineering. Retrieved from https://cs.lbl.gov/assets/CSSSP-Slides/20200625-Mueller.pdf. Assessed September 30, 2022.
- Nicolai, T., Britten, M., & Schmitt, C. (2011). β-Lactoglobulin and WPI aggregates: Formation, structure and applications. Food Hydrocolloids, 25, 1945–1962. https://doi.org/10.1016/j.foodhyd.2011.02.006
- Pathania, S., Bhatia, C., & Tiwari, B. K. (2021). Food formulation and product development. In S. Pathania, & B. K. Tiwari (Eds.), Vol. 1. Food formulation: Novel ingredients and processing techniques (pp. 1–4). John Wiley & Sons Ltd.. https://doi. org/10.1002/9781119614760
- Petit, J., Herbig, A.-L., Moreau, A., & Delaplace, G. (2011). Influence of calcium on β-lactoglobulin denaturation kinetics: Implications in unfolding and aggregation mechanisms. *Journal of Dairy Science*, 94, 5794–5810. https://doi.org/10.3168/ ids.2011-4470
- Purwanti, N., Smiddy, M., van der Goot, A. J., de Vries, R., Alting, A., & Boom, R. (2011). Modulation of rheological properties by heat-induced aggregation of whey protein solution. Food Hydrocolloids, 25, 1482–1489. https://doi.org/10.1016/j. foodbyd 2011.02.027
- Salley, D. S., Keenan, G. A., Long, D., Bell, N. L., & Cronin, L. (2020). A modular programmable inorganic cluster discovery robot for the discovery and synthesis of polyoxometalates. ACS Central Science, 6, 1587–1593. https://doi.org/10.1021/ acsceptsci.0c00415
- Schmitt, C., Bovay, C., Rouvet, M., Shojaei-Rami, S., & Kolodziejczyk, E. (2007). Whey protein soluble aggregates from heating with NaCl: Physicochemical, interfacial, and foaming properties. *Langmuir*, 23, 4155–4166. https://doi.org/10.1021/la0632575
- Schulz, E., Speekenbrink, M., & Krause, A. (2018). A tutorial on Gaussian process regression: Modelling, exploring, and exploiting functions. *Journal of Mathematical Psychology*, 85, 1–16. https://doi.org/10.1016/j.jmp.2018.03.001
- Schweidtmann, A. M., Clayton, A. D., Holmes, N., Bradford, E., Bourne, R. A., & Lapkin, A. (2018). Machine learning meets continuous flow chemistry: Automated optimization towards the Pareto front of multiple objectives. *Chemical Engineering Journal*, 352, 277–282. https://doi.org/10.1016/j.cej.2018.07.031
- Settles, B. (2009). Active learning literature survey. Computer Sciences Technical Report 1648. University of Wisconsin–Madison.
- Vardhanabhuti, B., & Foegeding, E. A. (1999). Rheological properties and characterization of polymerized whey protein isolates. *Journal of Agricultural and Food Chemistry*, 47, 3649–3655. https://doi.org/10.1021/jf981376n